Expression of the cancer-associated *DNA polymerase ε P286R* in fission yeast leads to translesion synthesis polymerase dependent hypermutation and defective DNA replication

Ignacio Soriano[1,2,9], Enrique Vazquez[3], Nagore De Leon[1,2]*, Sibyl Bertrand[1]*, Ellen Heitzer[4], Sophia Toumazou[1,5], Claire Palles[6], Chen-Chen Pai[5], Timothy Humphrey[5], Ian Tomlinson[2], Sue Cotterill[7], Stephen E. Kearsey[1,8]

[1] ZRAB, University of Oxford, 11a Mansfield Rd, Oxford, OX1 3SZ, UK.

[2] The Institute of Genetics and Cancer, University of Edinburgh, Western General Hospital Crewe Road, Edinburgh EH4 2XU, UK.

[3] Vascular Pathophysiology Department, Centro Nacional de Investigaciones Cardiovasculares (CNIC), 28029 Madrid, Spain.

[4] Institute of Human Genetics, Diagnostic & Research Center for Molecular BioMedicine, Medical University of Graz, Neue Stiftingtalstrasse 6, 8010 Graz, Austria.

[5] CRUK-MRC Oxford Institute for Radiation Oncology, Department of Oncology, University of Oxford, ORCRB, Roosevelt Drive, Oxford, OX3 7DQ, UK.

[6] Gastrointestinal Cancer Genetics Laboratory, Institute of Cancer and Genomic Sciences, College of Medical and Dental Sciences, University of Birmingham, Birmingham B15 2TT, UK

[7] St. George's, University of London, Cranmer Terrace, Tooting, London SW17 0RE.

[8] Corresponding author (stephen.kearsey@zoo.ox.ac.uk)

[9] Co-Corresponding author (ignacio.soriano@igmm.ed.ac.uk)

* Equal contribution

Short title: Analysis of Pol ε P286R hypermutation in fission yeast

Version 230321

ABSTRACT

Somatic mutations in the proofreading domain of the replicative DNA polymerase ε (*POLE*-exonuclease domain mutations, *POLE*-EDMs) are frequently found in colorectal and endometrial cancers and, occasionally, in other tumours. POLE-associated cancers typically display hypermutation, microsatellite stability and a unique mutational signature, with a predominance of C > A transversions in the context TCT. To understand better the contribution of hypermutagenesis to tumour development, we have modelled the most recurrent *POLE*-EDM (*POLE-P286R*) in *Schizosaccharomyces pombe*. Whole-genome sequencing analysis revealed that the corresponding *pol2-P287R* allele also has a strong mutator effect in vivo, with a high frequency of base substitutions and relatively few frameshift mutations. The mutations are equally distributed across different genomic regions, but they occur within an AT-rich context. The most abundant base-pair changes are TCT > TAT transversions and, in contrast to human mutations, TCG > TTG transitions are not elevated, likely due to the absence of cytosine methylation in fission yeast. The *pol2-P287R* variant has an increased sensitivity to elevated dNTP levels and DNA damaging agents, and shows reduced viability on depletion of the Pfh1 helicase. In addition, S phase is aberrant and RPA foci are elevated, suggestive of persistent ssDNA or DNA damage, and the *pol2-P287R* mutation is synthetically lethal with *rad3* inactivation, indicative of checkpoint activation. Significantly, deletion of genes encoding some translesion synthesis polymerases, most notably Pol κ, partially suppresses *pol2-P287R* hypermutation, indicating that polymerase switching contributes to this phenotype.

AUTHOR SUMMARY

Cancer is a genetic disease caused by mutations that lead to uncontrolled cell proliferation and other tumour properties. Defects in DNA repair or replication can lead to cancer development by increasing the likelihood that cancer-causing mutations will happen. Here we look at a pathogenic variant of a polymerase involved in genome replication (DNA polymerase □□□POLE-P286R). This variant is associated with highly mutated cancer genomes. By introducing this mutation into the polymerase □ gene of a model organism, fission yeast, we show that it causes a large increase in single base substitutions, scattered throughout the genome. The sequence context of mutations is similar in fission yeast and humans, suggesting that the yeast model is useful for understanding how POLE-P286R causes such a high mutation rate. Yeast POLE-P286R cells show slow chromosome replication, suggesting that the polymerase has difficulty in copying certain chromosomal regions. Yeast POLE-P286R cells become inviable when the concentration of dNTP building blocks for DNA synthesis is increased, probably because the mutation rate is pushed to an intolerable level. Interestingly, we find that specialised polymerases that are tolerant of DNA damage contribute to the high mutation rate caused by POLE-P286R. These findings have implications for the therapy of POLE-P286R tumours.

INTRODUCTION

In eukaryotes, nuclear DNA replication is carried out by three members of the B-family of DNA polymerases (Pols), Pols α, δ and ε, which function cooperatively to guarantee accurate and efficient genome duplication. Pol α synthesizes the primer to initiate DNA replication, allowing Pol ε and Pol δ to take over leading and lagging strand synthesis, respectively. Unlike Pol α, Pols ε and δ display high processivity and fidelity, being the only nuclear polymerases with functional 3'-5' exonuclease activity capable of correcting mistakes made during DNA synthesis [1, 2].

Pol ε is a large, four-subunit protein with critical roles in DNA replication and repair, cell cycle control and epigenetic inheritance (reviewed in [3]). In contrast to Pol δ, Pol ε is a highly processive enzyme even in the absence of accessory factors [4-6], and is perhaps the most accurate eukaryotic DNA polymerase [7, 8]. The high intrinsic processivity is due to the presence of a small domain in the catalytic subunit (Pol2) that allows Pol ε to encircle the nascent dsDNA [6, 9]. Another unique feature of Pol2 is the presence of a tyrosine (Y431 in *S. cerevisiae*) in the major groove of the nascent base-pair binding pocket, which may contribute to the fidelity of polymerisation [9].

Proofreading increases Pol ε replication accuracy by ~100-fold [7] and has an essential role in the maintenance of genomic stability. Mutations inactivating the exonuclease activity of Pol ε cause an increased mutation rate in both yeast [10] and mice, and lead to murine tumours in tissues with a high rate of cell turnover [11]. Recently, these findings were shown to be relevant to human cancer from large-scale studies of colorectal (CRC) and endometrial cancers (EC) [12-15]. This analysis revealed a subset of hypermutated microsatellite-stable (MSS) tumours with heterozygous somatic mutations in the exonuclease domain of Pol ε. A further study of sporadic ECs showed that somatic *Pol ε* exonuclease domain mutations (*POLE* EDMs) were present in about 7% of cases [16]. Subsequently, several thousand colorectal and endometrial tumour samples have been analysed, reporting more than 10 different *POLE* driver mutations [17, 18]. Current data suggest that somatic *POLE* proofreading domain mutations are present in 1-2% of CRCs and 7-12% of ECs, and less commonly in hypermutated tumours of the brain, pancreas, ovary, breast, stomach, lung and prostate [18, 19]. The most striking molecular characteristic in tumours harbouring many somatic *POLE* EDMs is their very high mutation rate, often exceeding 100 mutations/Mb. These mutations are predominantly single base substitutions and define a characteristic mutational pattern with a high proportion of C > A transversions in the context TCT, C > T transitions in the context TCG and T > G transversions in the context TTT, corresponding to COSMIC signatures 10 SBS10a and SBS10b [16, 20-22].

The amino-acids substituted in somatic *POLE* EDMs show a variable incidence rate (reviewed in [18, 19]), with *POLE-P286R* being the most frequent variant in colorectal and endometrial cancer [16, 21, 23], reaching a frequency of ~7% in early-onset colorectal cancer [24]. Heterozygous *Pole-P286R* mice develop malignant tumours of diverse lineages, which show very high mutation rates in the range of human malignancies [25]. This exceptional mutator phenotype presumably leads to a greater cancer risk due to mutations in driver genes, explaining the frequent occurrence of this variant in cancers.

The equivalent substitution (*pol2-P301R*) has been functionally validated in *S. cerevisiae*, showing an unusually strong mutator effect, and even in the heterozygous state the mutator effect is comparable with complete MMR deficiency [23]. Interestingly, budding yeast expressing *pol2-P301R* shows a mutation rate far higher than that of the exonuclease inactive variant (*Pol ε* exonull), suggesting that P286R must be able to increase the mutation rate through other processes other than proofreading deficiency alone [23, 26]. Curiously, the mutation rate of Pol2-P301R *in vitro* is less than that of Pol ε exonull, and is reported to have increased polymerase activity with the ability to extend mismatched primer termini. It is possible that this phenotype may result from the P286R mutation blocking the nascent DNA terminus from switching to the exonuclease site [27]. Nevertheless, the *S. cerevisiae pol2-P301R* holoenzyme still shows some exonuclease activity [26], while the human enzyme has been reported to have none [21].

Defects in polymerases may lead to increases in mutation rates by several mechanisms. In *S. cerevisiae,* an exonuclease null Pol δ mutant activates mutagenic repair via a checkpoint pathway that elevates dNTP levels, and this may be more important for accumulation of mutations than the proofreading defect *per se* [28]. The mechanism behind the mutator phenotype of the colon-cancer associated variant *POLD1-R689W* is similar in that yeast cells expressing Pol3-R696W (equivalent to *POLD1-R689W*) show a checkpoint-dependent increase in dNTP levels, similar to that seen with proofreading defective mutants [29]. This elevation of dNTP pools further increases the rate of Pol δ errors, thus forming a vicious circle and a similar mechanism has been suggested to explain the mutator phenotype due to error-prone DNA polymerase ε variants [30]. However it remains unknown whether dNTP pool levels are elevated in response to cancer-associated Pol ε variants.

An additional mechanism linking polymerase defects to an increased mutation rate involves translesion synthesis (TLS) polymerases. In *S. pombe*, Pol κ, and Pol ζ to a lesser extent, contribute significantly to the mutator phenotype of a strain expressing defective Pol α [31]. This study suggests that TLS polymerases are recruited in response to replication fork stalling or collapse, restarting

synthesis at the cost of an increased replicative mutation rate. However, Pol ζ is not responsible for the P286R hypermutation phenotype in *S. cerevisiae* [26].

In this study, we have characterized the impact of the P286R variant on genome-wide mutation and S phase execution in the fission yeast *Schizosaccharomyces pombe*. Furthermore, we studied the effect of increasing the mutation frequency in the viability of cells with high mutational burden. Finally, we addressed the contribution of TLS polymerases to hypermutation.

RESULTS

Fission yeast mimic of POLE-P286R has a strong mutator phenotype

P286 is invariant in all Pol ε orthologues, and is also conserved in Pol δ, T4 and RB69 bacteriophage polymerases (Fig. 1A). A fission yeast mimic of *POLE-P286R* (*pol2-P287R*) and an exonuclease deficient variant (*pol2-D276A/E278A,* [32] [33]) were constructed and *in vivo* mutation rates were measured by fluctuation analysis. Introduction of these mutations did not affect the steady state levels of the protein (Supplementary Fig. S1). The Pol2-P287R variant is also hypermutagenic in fission yeast, with a rate of mutation that is about 70 times higher than wild type and about 10-fold higher than the catalytically dead mutant (Fig. 1B), supporting the hypothesis that this change results in defects substantially more severe than loss of proofreading. Interestingly, mutation of the equivalent proline to arginine (P311R) in *S. pombe* Pol δ (Pol3/Cdc6) did not result in a hypermutating phenotype (Fig. 1B), possibly reflecting the different roles of Pol ε and Pol δ as leading and lagging strand polymerases.

To analyse further the rate and the spectrum of mutations, we undertook a ~200-generation mutation accumulation (MA) experiment followed by deep sequencing of genomic DNA from wild-type and mutant cells. On average, we identified 0.5, 9.5 and 394 single-base substitutions in the wild-type, *pol2-D276A/E278A* and *pol2-P287R* strains, respectively (Fig. 1C). Consistent with the fluctuation assay data, *pol2-P287R* cells have the highest rate of mutation, exceeding that of *pol2-D276A/E278A* mutant by more than 40 times (Fig. 1C). In addition, this hypermutator variant displayed a relative absence of indels (Fig. 1C), consonant with the microsatellite-stable (MSS) phenotype of *POLE* EDM tumours [16]. There was no genomic region particularly prone to P287R-induced mutations, which were equally distributed across the genome (Fig. 1D).

Fission yeast mutations induced by pol2-P287R broadly recapitulate mutations seen POLE-P286R cancer genomes

We next wished to compare the mutation spectra occurring in *POLE-P286R* human cancers and the equivalent mutant in fission yeast. First, we analysed whole-exome sequencing data from the TCGA colorectal and endometrial tumours harbouring the P286R variant. As expected, both groups of samples displayed very similar patterns, typified by C > A transversions in the context TCT, C > T transitions in the context TCG and T > G transversions in the context TTT (Fig. 2A), which is in accordance with the specific mutational spectrum of *POLE* EDMs [16, 20, 21].

We then compared the pattern of *pol2-P287R* mutations to the human spectra (Fig 2A, 2B upper panel). In consonance with human cancers, the most abundant mutations are C > A transversions in which the mutated cytosine is in the context TCT, although not to the same proportion as in the tumour genomes (Fig. 2A, B). In addition, the *pol2-P287R* cells recapitulate the most discriminating genomic alterations for human *POLE* mutations: CG to AT ≥ 20%; TA to GC ≥ 4%; CG to GC ≤ 0.6% [34]. More precisely, *pol2-P287R* cells present values of 33%, 15%, and 0% respectively (Fig. 2B and Supplementary Fig. S2). However, the lack of TCG > TTG transitions in the *pol2-P287R* spectrum is noteworthy. In humans, C > T transitions in a CpG base context are probably due to the deamination of 5-methylcytosine to thymine [35, 36] and/or mutant POLE synthesis across methylated cytosines situated on the leading strand [37], and the absence of 5-methylcytosine in fission yeast may explain these differences. Overall, these data suggest that fission yeast expressing P287R is a useful model for the human mutation.

Genome-wide estimates of mutation rates and mutational spectrum of wild-type *S. pombe* have been recently published [38, 39]. We used the base-substitution mutations from both studies to generate the mutational spectrum of the wild-type strain and we then compared it with the percentage of base substitutions identified in *pol2-P287R* cells (Fig. 2B). We found a prominent enrichment of C > A transversions in an NCT context and T > G transversions in an NTT context in the *pol2-P287R* mutant. In contrast, C > G transversions occurred with increased frequency in the wild-type cells, being completely absent in the mutant strain (Fig. 2B). This indicates that the Pol2-P287R polymerase is not simply amplifying the pattern of mutations found in wild-type cells.

Sequence-context determinants affect mutation rate variability

To establish if mutations are generated in preferred nucleotide contexts, we aligned 103 bp long sequences, encompassing the trinucleotides harbouring the mutations and their 50 bp flanking regions, and determined the nucleotide frequency for each position relative to the centre of the alignment in both the wild-type and *pol2-P287R* cells. Figure 2C showed a 10-12 bp long region flanking the mutations in the case of the *pol2-P287R* strain (top right panel), with strong asymmetry

in the frequency of adenine (A) and thymine (T) in the same DNA strand relative to the mismatch position. This asymmetric bias is absent in the region flanking wild-type mutations (top left panel). As a control, alignment of randomly selected 103 bp sequences along the *S. pombe* genome generated flat profiles, in which the nucleotide composition coincided with the average genome content (Fig 2C, bottom panels).

Given the AT-richness in the vicinity of *pol2*-P287 induced mutations, we looked at AT-rich regions in general to see to see if this sequence context is a factor in mutational probability in yeast and human genomes. Our results indicated that around 50% of these mutations are embedded in sequences 9-50 bp long with an AT-enrichment $\geq$ 80% both in the fission yeast *pol2-P287R* mutant and P286R cancers (Fig. 2D). However, differences were found in regions over 50 bp (AT $\geq$ 80%), with 14 and 2.6% of TCT > TAT transversions in yeast and human respectively (Fig. 2D), likely caused by the higher AT-content of the *S. pombe* genome [40]. Non-mutated TCT did not show this bias towards AT-rich environments (Supplementary Fig. S3). Overall, this suggests that the mutagenic mechanism due to *pol2-P287R* is distinct from that seen in wild-type cells.

Similarities between pol2-P287R mutational patterns and COSMIC signatures

To compare the mutational consequences of the human and yeast POLE286R variant, we first generated the mutational patterns of the wild-type and *pol2-P287R* strains and corrected for the difference in trinucleotide frequencies in the *S. pombe* genome and the human exome (Fig. 3A), as described in [41]. Then, to assess if any of the mutational patterns determined in this study could be related to one of the COSMIC mutational signatures, a cosine heatmap was generated using the MutationalPatterns package [42]. A cosine similarity of 0.80 was considered a threshold for “high” similarity [41]. The *pol2-P287R* strain showed the highest similarity of 0.85 to the signature 14 (Fig. 3B and Supplementary Table S3). Signature 14 was previously established as linked with concurrent *POLE* EDM and defective MMR. The wild-type strain did not exhibit any cosine coefficient over the threshold, displaying a highest similarity of 0.72 to COSMIC signature 40 (Fig. 3B and Suppl. Table S3). This is currently a signature of unknown aetiology, although numbers of mutations attributed to it are correlated with patients’ ages for some types of human cancer. Moreover, these data indicate that the signature 10 associated with *POLE* EDMs in human cancers is not the most prevalent mutational pattern detected in the *pol2-P287R* strain. This may suggest that the mutational process in *S. pombe* *pol2-P287R* does not fully represent the situation in human cells. However it should be borne in mind that human cancer cells are heterozygous for the *POLE-P286R* mutation, while the *pol2-P287R*

mutation accumulation experiment used a haploid strain, so the mutagenic burden on mismatch repair would have been greater in the yeast strain.

pol2-P287R cells exhibit increased sensitivity to DNA-damaging agents

Cells with a high rate of spontaneous mutations frequently display increased sensitivity to DNA-damaging agents [43, 44]. Furthermore, Pol ε is implicated in various repair pathways [3].To gain further insight into this relationship, we performed spot assay analyses in the presence of different mutagenic agents. Results showed that *pol2-P287R* cells are very sensitive to agents inducing DNA breaks, such as bleocin, or nucleotide modification, such as MMS, 4-NQO, UV radiation, but not to HU, a ribonucleotide reductase inhibitor (Fig. 4A). In fact, *pol2-P287R* cells showed some resistance to HU. The sensitivity to MMS is particularly dramatic and maybe due to the fact that, at the concentrations used, this alkylating agent generates 25 and 50-fold more lesions than 4-NQO and bleocin, respectively [45]. The sensitivity of *pol2-P287R* to DNA damaging agents is seen with several independently derived strains, so it is unlikely that this phenotype is due to second-site mutations facilitated by the strain's hypermutation. Given the sensitivity to a wide range of DNA damaging agents, it is possible that Pol2-P287R compromises the ability of the replication fork to cope with damaged template, rather than an effect on a specific repair pathway.

Increased dNTP levels lead to lethality in pol2-P287R cells

As described above, *pol2-P287R* cells exhibit slight resistance to HU (Fig. 4A), suggesting that this mutant could have increased dNTP pools under normal conditions. Increased dNTP levels can elevate the mutation rate and, in combination with genetic alterations affecting DNA polymerase nucleotide selectivity, proofreading activity, or MMR, cause enhanced mutator phenotype ([29, 30, 46] reviewed in [47]). However, the *pol2-P287R* strain showed similar levels of dNTPs to wild-type and *pol2-exonull* cells (Fig. 4B), indicating that dNTP alterations are not contributing to its hypermutagenic phenotype.

Increased dNTP levels are detrimental to the fidelity of DNA replication in bacteria, yeast and mammalian cells (reviewed in [47]. This effect might be exacerbated in the case of the error-prone Pol2-P287R variant. To address this possibility, we crossed a *cdc22-D57N* strain, where dNTP levels are enhanced due to inactivation of ribonucleotide reductase allosteric regulation, with the exonuclease-deficient *pol2-D276A/E278A* and *pol2-P287R* mutants and analysed the progeny by tetrad dissection. Double *pol2-D276A/E278A cdc22-D57N* mutants were readily obtained but the double *pol2-P287R cdc22-D57N* were not, implying synthetic lethality (Fig. 4C). The mutation burden of the *pol2-P287R* strain could be near the limit of the 'error-induced extinction', and an increase in

the mutation frequency caused by raised dNTP levels may be sufficient to dramatically decrease the fitness of these cells, but this is tolerated in the *pol2-D276A/E278A* control, which has a lower mutation rate.

The pol2-P287R mutation causes S phase defects and is dependent on Rad3 for viability

We noticed that a proportion of *pol2-P287R* cells were elongated (Supplementary Fig. S4), and the doubling time of the strain is longer than wild-type or exonull strains (Fig. 5A), suggesting that problems with S phase might lead to a mitotic delay via checkpoint activation. To investigate this in more detail, cells were arrested in G1 by nitrogen starvation, released from the block and flow cytometry was used to follow the progress of S phase. This showed a slower completion of S phase in the *pol2-P287R* strain (Fig. 5B) compared to wild-type cells, while the wild-type and exonull strains showed similar S phase kinetics. To examine S phase execution by a different method, we pulsed cells with EdU for 15 minutes and measured the length of replication tracts by DNA combing (Fig 5C,D). The *pol2-P287R* cells showed shorter incorporation tracks, suggesting that fork progression is slower, or fork stalling is more frequent.

To determine if the Rad3 checkpoint kinase is required for viability of the *pol2-P287R* cells, we made double mutants with a temperature-sensitive *rad3ts* allele. While the exonuclease null double mutant was viable at the restrictive temperature, the *pol2-P287R* double mutant was not (Fig. 5E). We also found that foci of Rad11-GFP, a subunit of RPA, were more common in *pol2-P287R* cells compared to wild-type and exonull strains, suggesting that single-stranded DNA and perhaps DNA damage may result from replication by the mutant polymerase (Fig. 5F, Supplementary Fig. S5). Consistent with these observations, we observed a low level of Chk1 and Cds1 phosphorylation in the *pol2-P287R* mutant (Fig 5G, H). Taken together, these observations suggest that a slower, defective S phase and accumulation of single-stranded DNA results from replication by Pol2-P287R, resulting in partial activation of the DNA damage and replication checkpoints.

Genetic interaction with Pfh1 helicase

Given our observations that Pol2-P287R results in a defective S phase, we investigated whether there is a genetic interaction with Pif1/Pfh1 helicase, since this enzyme is involved in replicating through template barriers such as transcription complexes [48-50]. In *S. pombe*, Pfh1 has an essential role in the maintenance of both nuclear and mitochondrial DNA [51]. Therefore, to study its genetic interaction with the exonuclease variants, we made double mutants of *pol2-P287R* with a conditional allele of *pfh1 (nmt1-81Xpfh1-GFP)*, where the gene is under the control of a weak promoter that is

down-regulated by thiamine [51]. In the absence of thiamine, Pfh1 is localized to the nucleus and mitochondria (Fig 6, top panels) and all the strains grew well at 26°, 30° and 36° C (Fig. 7B, top panels). The nuclear signal is dramatically reduced in the presence of thiamine (Fig 7A, bottom panels). The growth of the *pol2-D276A/E278A nmt1-81Xpfh1-GFP* double mutant strain was similar to wild-type, when *pfh1-GFP* was repressed. However, *pol2-P287R nmt1-81Xpfh1-GFP* cells were very sick suggesting a strong genetic interaction with *pfh1* (Fig. 7B).

It has been recently found that Pfh1 overexpression is able to rescue some replication defects in fission yeast [52]. We wondered whether Pol2-P287R defects could be partially alleviated by overexpressing this helicase. *pol2-287R* cells were transformed with pREP1 plasmid expressing Pfh1 DNA helicase under the control of the full strength (3X) *nmt1* promoter and spot assays were performed. Results indicated that overexpression of Pfh1 largely suppresses some defective phenotypes of *pol2-P287R* mutant cells, such as the growth defects at 30° C in minimal medium and the sensitivity to MMS (Fig. 7C). However, the 4-NQO sensitivity was not rescued by the overexpression of the helicase. Overall, these results suggest that the replisome in *pol2-P287R* cells may have difficulty in dealing with 'hard-to-replicate' template particularly if Pfh1 levels are low, but enhanced Pfh1 activity may to some extent compensate for *pol2-P287R* defects.

Pol κ deletion suppresses the hypermutagenic phenotype

In contrast to its strong mutator effect *in vivo*, it has been shown in *S. cerevisiae* that P286R does not have a high error rate *in vitro* [26]. We hypothesized that as a consequence of the failed proofreading caused by the *pol2-P287R* mutation, replication fork stalling might increase and TLS polymerases could be recruited onto chromatin, to extend mismatched primer terminus, resulting in mutagenic synthesis [31]. We analysed the mutation rates of different TLS polymerase mutants containing a deletion of *rev1*, *rev3* (the catalytic domain of Pol ζ) or *kpa1* (Pol κ), or a single point mutation in *eso1* (*eso1-D147N*) inactivating Pol η, individually and in combination with *pol2-P287R*. Canavanine fluctuation assays showed that deletion of *rev3* in *pol2-P287R* cells did not significantly change the error rate (Fig. 7A), consistent with data from *S. cerevisiae* [26]. In the case of *rev1*Δ *pol2-P287R* and *eso1-D147N pol2*-P287R double mutants, the error rate was partially decreased (Fig. 7A). Strikingly, *kpa1* deletion reduced the mutation rate of *pol2-P287R* to a level similar to an exonuclease deficient mutant, suggesting that this polymerase contributes to mutagenesis in cells expressing Pol2-P287R.

To confirm this result, we performed a ~200-generation mutation accumulation (MA) experiment followed by deep sequencing of genomic DNA from *kpa1*Δ and *eso1-D147N* single and double mutants. Sequencing data showed a reduction of around 4-fold in the number of mutations

accumulated in the absence of Pol η activity compared to the single *pol2-P287R* mutant. In accordance with the fluctuation rate assays, *kpa1*Δ caused a stronger reduction in the mutation burden, with a 15-fold decrease in the number of mutations accumulated the *kpa1*Δ *pol2-P287R* double mutant (Fig. 7B). Overall, these results suggest that an important feature of hypermutation caused by the *pol2-P287R* variant is polymerase switching to TLS polymerases.

DISCUSSION

Defects in DNA replication have long been suggested to have a causative role in human cancer, but specific examples have only recently emerged. Recently, several studies show that somatic *POLE* proofreading domain mutations occur in sporadic ECs, CRCs and several other cancers (reviewed in [18, 19]) The *POLE* EDMs are associated with a phenotype of hypermutation, microsatellite stability and favourable prognosis, possibly due to T cell responses to tumour neoantigens [53]. The most frequent variant, P286R, has been modelled in *S. cerevisiae* (Pol2-P301R), where it causes a strong mutator effect even in the heterozygous condition, in excess to that seen with exonuclease defective Pol2. [23]. However, the mechanisms leading to this hypermutation phenotype are not well understood.

Our results show that the equivalent mutation of *POLE-P286R*, *pol2-P287R*, is also highly mutagenic in fission yeast, with a base substitution frequency much higher than that caused by loss of the exonuclease activity of Pol ε. In consonance with findings in human cancers, the most abundant mutation is a C > A transversion in a TCT context, although the mutational pattern in yeast does not completely mirror the human pattern. The mutational pattern is not just a reflection of the polymerase defect, since it is also affected by mismatch repair, which may differ in its specificity and efficiency between yeast and humans. In addition, the *pol2-P287R* mutant shows reduced S phase kinetics, sensitivity to DNA damaging agents, increased RPA foci, dependence on Rad3, and a low level of Chk1 and Cds1 phosphorylation, indicating partial activation of the DNA damage and replication checkpoints. The human *POLE-P286R* mutation is found in the heterozygous condition, so we would not predict tumour cells carrying this mutation would necessarily show an S phase delay. Indeed mice heterozygous for the P286R are born healthy and fertile, with no enhancement of DNA damage markers although they are highly cancer prone [54]. In contrast, mice hemizygous for the *POLE-P286R* mutation generally show embryonic lethality. Thus mammalian cells heterozygous for the *POLE-P286R* mutation may be ideally predisposed for cancer formation, having a sufficiently high mutation rate but without defects in cell cycle progression.

Budding yeast Pol2-P301R has a lower mutation rate than Pol2-exonull in vitro [26], so it is not clear what is responsible for the high *in vivo* mutation rate. One suggestion is that the strong mutator effect results from higher polymerase activity and more efficient mismatch extension capacity, which leads to misincorporation rather than proofreading [26]. Our data suggest that additional mechanisms are involved, namely that Pol κ, and to a lesser extent Pol η, contributes to the elevated mutation rate of the *pol2-P287R* mutant, similar to the situation seen with defective Pol α [31]. Pol κ, and less so Pol η, are efficient at extending from a mismatch [55, 56], and show error rates considerably higher than Pols δ and ε [56]. Pol κ has also been implicated in restart of stalled replication forks [57]. Previous work has suggested that following misincorporation, the budding yeast Pol2-P301R has a tendency to extend the mismatch [26], but the ability of Pol δ to proofread Pol2-P301R errors means that the enzyme must dissociate some of the time [58]. We suggest that in this situation, Pols κ and η may compete with Pol δ for extension of the leading strand, leading to mutagenic synthesis (Supplementary Fig. S6). Interestingly, our data show that mutation of the proline equivalent to P286 in Pol δ does not lead to hypermutation, consistent with the fact that tumour sequencing has not identified this as a clinical mutation. Displacement of the lagging strand polymerase may simply lead to downstream initiation of an Okazaki fragment, and thus no polymerase switching.

In addition to their roles in lesion bypass during translesion synthesis, Pols κ and η have important functions during the replication of hard-to-replicate sites such as microsatellite sequences, G-quadruplex and common fragile sites (CFSs), and during conditions of replicative stress [59]. Pol ε P287R may be more prone to stalling or displacement at such sequences compared to wild-type or exonull polymerases, as suggested by the interaction with Pfh1 reported here, perhaps again allowing exchange with Pol κ.

POLE proofreading domain-mutant tumours may be particularly sensitive to specific therapeutic approaches due to their exceptional mutation burden. One strategy to decrease the overall fitness of hypermutating tumour cells is by increasing the mutation frequency further to induce an error catastrophe, similar to lethal mutagenesis of viruses [60]. Indeed, we found that *pol2-P287R* cells are sensitive to high dNTP levels, which probably reflects a further increase in mutation rate leading to cell death by error-induced catastrophe. Normal somatic cells might be much less sensitive to a transient increase in mutation rate [60, 61]. Clinically, an increase in the mutation rate could be effected by, for instance, decreasing the efficiency of MMR, or inducing DNA lesions using DNA damaging agents or nucleoside analogues. Additionally, upregulating RNR or inactivating SAMHD1

would also increase dNTP levels. Interestingly, SAMHD1 putative cancer drivers [62] are not found in any of the POLE-P286R tumours from a collection containing 2188 non-redundant samples from 10 colorectal and endometrial studies [63, 64], suggesting that these mutations might be mutually exclusive.

In conclusion, while previous work has focused on features of POLE P286R function that are intrinsic to the enzyme, our results in *S. pombe* suggest that some aspects the high mutagenesis is a result of in vivo responses to polymerase malfunction. Clearly it will be of interest to see a similar situation is also found in human cells.

Materials and methods

S. pombe methods

Standard media and genetic techniques were used as previously described [65]. Cultures were grown in either rich medium (YE3S), or Edinburgh minimal medium (EMM) supplemented with the appropriate requirements and incubated at 30°C with shaking, unless otherwise stated. Nitrogen starvation was carried out using EMM lacking NH_4Cl. The relevant genotypes and source of the strains used in this study are listed in Table S1. Oligos used for strain constructions are listed in Table S2.

For spot testing, cells were grown overnight to exponential phase and five serial dilutions (1/4) of cells were spotted on agar plates using a replica plater (Sigma R2383). Plates were incubated at the relevant temperature, and photographed after 2-3 days.

Growth curves were obtained using the Bioscreen C MBR machine. Cultures in exponential phase were adjusted to 2 x 10^6 cells/ml and 250 µl were dispensed in 4-8 replicate wells for each strain. The plate was incubated at 30°C with constant shaking at maximum amplitude. The OD600 of each well was measured every 20 minutes for 22 hours. Duplication time was determined via analysis of the exponential phase of the plotted log2 graph time vs OD600 using the exponential growth equation available on Prism.

Cell lengths were determined using an AxioPlan 2 microscope and pictures where taken using a Hamamatsu ORCA E camera system with Micro-Manager 1.3 software. Cell length was measured

using ImageJ. Fluorescence microscopy was carried out as previously described [66], except cells were not fixed.

dNTP levels were determined as previously described [67].

S. pombe pol2 variant strains were constructed as described previously [68]. The *pol2-P287R* strain was constructed using mutagenic primers 1128 and 1129; the P>R mutation generates an NruI site.

S. pombe pol3 variant strains were constructed as previously described [69]. For strain *pol3P311R::kanMX6* (3419), mutagenic primers used were 1192 and 1193, with flanking primers 1148 and 1076. The mutation introduces a NruI site. The final PCR product was cloned into pFA6a as AscI-BamHI fragment and integrated at the *pol3* locus after cleavage with XhoI. The exonull strain *pol3D386A* was based on the mouse D400A mutation which has been shown to lack exonuclease activity. [70]. Mutagenic primers used were 1140 and 1141, with flanking primers 1075 and 1076; the mutation also introduces a NruI site. The final PCR product was cloned as above and integrated into the *pol3* locus after cleavage with CspCI.

Protein analysis

Proteins were extracted by TCA method and resolved on 3-8% Tris Acetate NuPAGE (Thermo Scientific) in reducing conditions (NuPAGE Tris Acetate SDS running buffer – Thermo Scientific) [71]. For analysis of Chk1 and Cds1 phosphorylation, cells were grown to log phase in YES at 30°C. As a positive control for Chk1 phosphorylation, cells were grown YES plus 0.025% MMS. As a positive control for Cds1 phosphorylation, cells were grown YES plus 10 mM hydroxyurea. In the case of P-Chk1 analysis, proteins were resolved by SDS-PAGE using 10% gels with an acrylamide/bisacrylamide ratio of 99:1 [72]. Phos-tag acrylamide gels (Wako) were used to detect Cds1-P. Proteins were transferred onto a PVDF membrane by a dry transfer method using the iBlot2 Dry Blotting System (Thermo Fisher Scientific). Every step from blocking to washes to antibody incubation was performed via sequential lateral flow with the iBind Flex Western device. HA-tagged proteins were detected with the rabbit monoclonal antibody HA-Tag (C29F4). The secondary anti-rabbit used was Dako PO448. α tubulin was used as a loading control and the probing was done by using mouse monoclonal anti-α-tubulin (Sigma T5168). The secondary antibody used was goat anti-mouse (HRP) Ab97040.

Mutation accumulation experiments

Strains were woken up from -70°C, then single colonies were used to start lineages. One colony was grown up to prepare DNA for sequencing (generation 0) and restreaked on a fresh YES plate. After the colonies had grown up (3 days), a single colony was restreaked on a second YES plate. This process was repeated until the cells had gone through approximately 200 generations (11 passages). At the end of the experiment a single colony was grown up to prepare DNA for sequencing (generation 200). Variants were called (see sequencing analysis) and mutations were identified if present in generation 200 DNA but not in generation 0 DNA. Doubling time used to estimate the number of generations, as previously described [39].

Mutation rate analysis by fluctuation analysis

Mutation to canavanine resistance was used to estimate mutation rates, as previously described (Kaur et al., 1999). A culture (10^4 cells/ml) was aliquoted into 12 wells of a 96-well microtitre plate (0.25 ml/well) and allowed to grow to saturation. Dilutions were plated onto YES plates to determine the cell concentration, and 0.15 ml of each culture was plated out onto a PMG plate (EMM-G, (Fantes and Creanor, 1984)) containing 80 μg/ml canavanine. Canavanine-resistant colonies were counted after 11 days at 30°C. Mutation rates were calculated using the Ma-Sandri-Sarkar maximum likelihood estimator (Sarkar et al., 1992), implemented in rSalvador (Zheng, 2017).

Sequencing analysis

Libraries were sequenced on a HiSeq2500 (Illumina) to generate 2x150 bases paired reads with an average genome coverage of ~200-fold and processed with RTA v1.18.66.3. FastQ files for each sample were obtained using bcl2fastq v2.20.0.422 software (Illumina). More than 6.5 M of pairs per sample were obtained. QC check of sequencing reads were revised with FastqC software and, then reads were trimmed off Illumina adapters using Cutadapt 1.16. Trimmed fastq file were aligned to *S. pombe* reference genome (ASM294v2.20 assembly) using Bowtie 2 with '--fr -X 1000 -I 0 -N 0 --local -k 1' parameters. Sequencing duplicate read alignments were excluded using MarkDuplicates and sorted using Samtools. For bigwig (bw) representation and visual inspection bamCoverage and IGV software were used.

For the variant calling process, the bam files were processed with mpileup from Samtools and the calling process were executed with VarScan2. For somatic variant calling VarScan2 was used with both Generation 0 (G0) and Generation 200 (G200) mpileup file and only the High Confident (HC)

variants were retained for next analysis. Human variant calling files from colorectal and endometrial POLE-P286R cancers were obtained from the cBioPortal curated set of non-redundant studies [63, 64]. To calculate the consensus variants (both in *S. pombe* and human variants) of a genotype we retained SNPs from different genome positions and, for the same position, only when the same change occurs in all variant files. All secondary analyses were made with custom python scripts available under request.

Sequencing data from this study have been deposited in the Gene Expression Omnibus (GEO) database under the accession number GSE169231 (https://www.ncbi.nlm.nih.gov/geo/query/acc.cgi?acc=GSE169231).

Bioinformatic analysis

Genomic region annotation data (Fig. 1D) were derived from the *S. pombe* reference genome (ASM294v2.20 assembly). The 'expected' values correspond to the percentage of each genomic region across the genome. To determine the 'observed' distribution, the number of substitutions at each genomic region were calculated using a custom Python script and percentages represented.

To establish the base substitution patterns of POLE-P286R colorectal and endometrial cancer, tsv files corresponding to CRC and UEC samples harbouring *POLE-P286R* mutation were downloaded from cBioportal [63, 64] and the average percentage of single mutations across all individual samples per cancer type in their 5' and 3' base sequence context calculated and plotted using a custom Python script (Figure 2A). For the mutational patterns in fission yeast, 1073 and 746 single base substitutions from the P287R (this study) and WT [38, 39] MA experiments respectively were identified and plotted as above (Figure 2B).

For determining base composition in the vicinity of mutations (Fig. 2C) 103 bp long DNA sequences harbouring single base substitutions were aligned to the mismatched position. The percentage of mononucleotides were calculated for each position. Alignment of the same number of sequences 103-bp long randomly selected along the *S. pombe* genome were used as a control.

A + T content of regions harbouring TCT > TAT transversion ranging from 9-20 bp, 21-50 bp and >50 bp (Figure 2D) was calculated using *S. pombe* or human GRCh37 reference genomes for *pol2-P287R* and P286R-CRC/P286R-UEC samples respectively.

Base substitution patterns of the wild-type and *pol2-P287R* strains (Figure 2B) were normalized by the trinucleotide frequencies in the fission yeast genome to generate the corresponding mutational

patterns. The latter were then corrected for the difference in trinucleotide frequencies in the *S. pombe* genome and the human exome to establish the humanized versions (Figure 3A), as previously described [41].

Cosine similarity values for the comparison between humanized *S. pombe* mutation patterns with COSMIC v3.1 signatures (both adjusted to human whole-exome trinucleotide frequencies) were calculated using the Python cosine_similarity script from Scikit-learn [73].The heat map (Fig. 3B) was generated using Morpheus software (Morpheus, https://software.broadinstitute.org/morpheus)

Flow cytometry

Cells were fixed in 70% ethanol and analysed after RNase digestion and SYTOX Green staining as previously described [74].

DNA combing

DNA combing was carried out basically as previously described [75, 76], using a Genomic Vision Molecular Combing system and CombiCoverslips.. A pulse of 100 μM EdU for 15 minutes was used to label DNA and incorporated EdU was detected using AlexaFluor 488 Azide A10266 (ThermoFisher Scientific) A10266.

Acknowledgements

This work was supported by the Medical Research Council (grant MR/L016591/1 to SC and SEK) and the European Research Council (EVOCAN grant 340560 to Ian Tomlinson). We are grateful to Catherine Green and Jane Mellor for providing lab facilities following the abrupt closure of the Tinbergen building in February 2017. We thank Tony Carr, Stéphane Coulon, Christian Holmberg, Edgar Hartsuiker, Paul Russell, Virginia Zakian and NBRP Japan for strains or plasmids. We are grateful to Philippe Pasero providing facilities and guidance regarding DNA combing.

References

1. Garg P, Burgers PMJ. DNA Polymerases that Propagate the Eukaryotic DNA Replication Fork. Critical Reviews in Biochemistry and Molecular Biology. 2005;40(2):115-28. doi: 10.1080/10409230590935433.
2. Johnson A, O'Donnell M. CELLULAR DNA REPLICASES: Components and Dynamics at the Replication Fork. Annual Review of Biochemistry. 2005;74(1):283-315. doi: 10.1146/annurev.biochem.73.011303.073859.
3. Pursell ZF, Kunkel TA. DNA polymerase epsilon: a polymerase of unusual size (and complexity). Prog Nucleic Acid Res Mol Biol. 2008;82:101-45. Epub 2008/10/22. doi: 10.1016/S0079-6603(08)00004-4. PubMed PMID: 18929140; PubMed Central PMCID: PMCPMC3694787.
4. Bermudez VP, Farina A, Raghavan V, Tappin I, Hurwitz J. Studies on human DNA polymerase epsilon and GINS complex and their role in DNA replication. The Journal of biological chemistry. 2011;286(33):28963-77. doi: 10.1074/jbc.M111.256289.
5. Dua R, Levy DL, Li CM, Snow PM, Campbell JL. In vivo reconstitution of Saccharomyces cerevisiae DNA polymerase epsilon in insect cells. Purification and characterization. The Journal of biological chemistry. 2002;277(10):7889-96. doi: 10.1074/jbc.M108546200.
6. Hogg M, Osterman P, Bylund GO, Ganai RA, Lundström E-B, Elisabeth Sauer-Eriksson A, et al. Structural basis for processive DNA synthesis by yeast DNA polymerase ε. Nature Publishing Group. 2013;21(1). doi: 10.1038/nsmb.2712.
7. Shcherbakova PV, Pavlov YI, Chilkova O, Rogozin IB, Johansson E, Kunkel TA. Unique error signature of the four-subunit yeast DNA polymerase epsilon. J Biol Chem. 2003;278(44):43770-80. Epub 2003/07/29. doi: 10.1074/jbc.M306893200. PubMed PMID: 12882968.
8. Thomas DC, Roberts JD, Sabatino RD, Myers TW, Tan CK, Downey KM, et al. Fidelity of mammalian DNA replication and replicative DNA polymerases. Biochemistry. 1991;30(51):11751-9.

9. Jain R, Rajashankar KR, Buku A, Johnson RE, Prakash L, Prakash S, et al. Crystal Structure of Yeast DNA Polymerase ε Catalytic Domain. PLoS ONE. 2014;9(4):e94835-e. doi: 10.1371/journal.pone.0094835.
10. Morrison A, Bell JB, Kunkel TA, Sugino A. Eukaryotic DNA polymerase amino acid sequence required for 3'----5' exonuclease activity. Proc Natl Acad Sci U S A. 1991;88(21):9473-7. Epub 1991/11/01. doi: 10.1073/pnas.88.21.9473. PubMed PMID: 1658784; PubMed Central PMCID: PMCPMC52740.
11. Albertson TM, Ogawa M, Bugni JM, Hays LE, Chen Y, Wang Y, et al. DNA polymerase epsilon and delta proofreading suppress discrete mutator and cancer phenotypes in mice. Proceedings of the National Academy of Sciences of the United States of America. 2009;106(40):17101-4. doi: 10.1073/pnas.0907147106.
12. Getz G, Gabriel SB, Cibulskis K, Lander E, Sivachenko A, Sougnez C, et al. Integrated genomic characterization of endometrial carcinoma. Nature. 2013;497(7447):67-73. doi: 10.1038/nature12113.
13. Network TCGA. Comprehensive molecular characterization of human colon and rectal cancer. Nature. 2012;487(7407):330-7. doi: 10.1038/nature11252.
14. Seshagiri S, Stawiski EW, Durinck S, Modrusan Z, Storm EE, Conboy CB, et al. Recurrent R-spondin fusions in colon cancer. Nature. 2012;488(7413):660-4. doi: 10.1038/nature11282.
15. Mur P, Garcia-Mulero S, Del Valle J, Magraner-Pardo L, Vidal A, Pineda M, et al. Role of POLE and POLD1 in familial cancer. Genet Med. 2020;22(12):2089-100. Epub 2020/08/15. doi: 10.1038/s41436-020-0922-2. PubMed PMID: 32792570; PubMed Central PMCID: PMCPMC7708298.
16. Church DN, Briggs SEW, Palles C, Domingo E, Kearsey SJ, Grimes JM, et al. DNA polymerase ε and δ exonuclease domain mutations in endometrial cancer. Human Molecular Genetics. 2013;22(14):2820-8. doi: 10.1093/hmg/ddt131.
17. Hu H, Cai W, Wu D, Hu W, Dong Wang L, Mao J, et al. Ultra-mutated colorectal cancer patients with POLE driver mutations exhibit distinct clinical patterns. Cancer Med. 2021;10(1):135-42. Epub 2020/10/31. doi: 10.1002/cam4.3579. PubMed PMID: 33125191.
18. Rayner E, van Gool IC, Palles C, Kearsey SE, Bosse T, Tomlinson I, et al. A panoply of errors: polymerase proofreading domain mutations in cancer. Nat Rev Cancer. 2016;16(2):71-81. Epub 2016/01/30. doi: 10.1038/nrc.2015.12. PubMed PMID: 26822575.
19. Barbari SR, Shcherbakova PV. Replicative DNA polymerase defects in human cancers_ Consequences, mechanisms, and implications for therapy. DNA Repair. 2017:1-10. doi: 10.1016/j.dnarep.2017.06.003.
20. Alexandrov LB, Nik-Zainal S, Wedge DC, Aparicio SAJR, Behjati S, Biankin AV, et al. Signatures of mutational processes in human cancer. Nature. 2013;500(7463):415-21. doi: 10.1038/nature12477.
21. Shinbrot E, Henninger EE, Weinhold N, Covington KR, Goksenin AY, Schultz N, et al. Exonuclease mutations in DNA polymerase epsilon reveal replication strand specific mutation patterns and human origins of replication. Genome Res. 2014;24(11):1740-50. Epub 2014/09/18. doi: 10.1101/gr.174789.114. PubMed PMID: 25228659; PubMed Central PMCID: PMCPMC4216916.
22. Alexandrov LB, Kim J, Haradhvala NJ, Huang MN, Tian Ng AW, Wu Y, et al. The repertoire of mutational signatures in human cancer. Nature. 2020;578(7793):94-101. Epub 2020/02/07. doi: 10.1038/s41586-020-1943-3. PubMed PMID: 32025018; PubMed Central PMCID: PMCPMC7054213.

623 23. Kane DP, Shcherbakova PV. A common cancer-associated DNA polymerase epsilon
624 mutation causes an exceptionally strong mutator phenotype, indicating fidelity defects
625 distinct from loss of proofreading. Cancer Res. 2014;74(7):1895-901. Epub 2014/02/15. doi:
626 10.1158/0008-5472.CAN-13-2892. PubMed PMID: 24525744; PubMed Central PMCID:
627 PMCPMC4310866.
628 24. Ahn S-M, Adnan Ahmad A, Kim J, Kim D, Chun S-M, Kim J, et al. The somatic POLE
629 P286R mutation defines a unique subclass of colorectal cancer featuring hypermutation,
630 representing a potential genomic biomarker for immunotherapy. Oncotarget.
631 2016;7(42):68638-49. doi: 10.18632/oncotarget.11862.
632 25. Li HD, Cuevas I, Zhang M, Lu C, Alam MM, Fu YX, et al. Polymerase-mediated
633 ultramutagenesis in mice produces diverse cancers with high mutational load. J Clin Invest.
634 2018;128(9):4179-91. Epub 2018/08/21. doi: 10.1172/JCI122095. PubMed PMID: 30124468;
635 PubMed Central PMCID: PMCPMC6118636.
636 26. Xing X, Kane DP, Bulock CR, Moore EA, Sharma S, Chabes A, et al. A recurrent cancer-
637 associated substitution in DNA polymerase ε produces a hyperactive enzyme. Nature
638 Communications. 2019;10(1):374-. doi: 10.1038/s41467-018-08145-2.
639 27. Parkash V, Kulkarni Y, Ter Beek J, Shcherbakova PV, Kamerlin SCL, Johansson E.
640 Structural consequence of the most frequently recurring cancer-associated substitution in
641 DNA polymerase epsilon. Nat Commun. 2019;10(1):373. Epub 2019/01/24. doi:
642 10.1038/s41467-018-08114-9. PubMed PMID: 30670696; PubMed Central PMCID:
643 PMCPMC6342957.
644 28. Datta A, Schmeits JL, Amin NS, Lau PJ, Myung K, Kolodner RD. Checkpoint-Dependent
645 Activation of Mutagenic Repair in Saccharomyces cerevisiae pol3-01 Mutants. Molecular
646 Cell. 2000;6(3):593-603. doi: 10.1016/S1097-2765(00)00058-7.
647 29. Mertz TM, Sharma S, Chabes A, Shcherbakova PV. Colon cancer-associated mutator
648 DNA polymerase δ variant causes expansion of dNTP pools increasing its own infidelity.
649 Proceedings of the National Academy of Sciences of the United States of America.
650 2015;112(19):E2467-76. doi: 10.1073/pnas.1422934112.
651 30. Williams LN, Marjavaara L, Knowels GM, Schultz EM, Fox EJ, Chabes A, et al. dNTP
652 pool levels modulate mutator phenotypes of error-prone DNA polymerase ε variants.
653 Proceedings of the National Academy of Sciences of the United States of America.
654 2015;112(19):E2457-66. doi: 10.1073/pnas.1422948112.
655 31. Kai M, Wang TSF. Checkpoint activation regulates mutagenic translesion synthesis.
656 Genes & development. 2003;17(1):64-76. doi: 10.1101/gad.1043203.
657 32. Pursell ZF, Isoz I, Lundstrom EB, Johansson E, Kunkel TA. Regulation of B family DNA
658 polymerase fidelity by a conserved active site residue: characterization of M644W, M644L
659 and M644F mutants of yeast DNA polymerase. Nucleic Acids Research. 2007;35(9):3076-86.
660 doi: 10.1093/nar/gkm132.
661 33. Korona DA, LeCompte KG, Pursell ZF. The high fidelity and unique error signature of
662 human DNA polymerase. Nucleic Acids Research. 2011;39(5):1763-73. doi:
663 10.1093/nar/gkq1034.
664 34. León-Castillo A, Britton H, McConechy MK, McAlpine JN, Nout R, Kommoss S, et al.
665 Interpretation of somatic POLE mutations in endometrial carcinoma. The Journal of
666 Pathology. 2020;250(3):323-35. doi: 10.1002/path.5372.
667 35. Fang H, Barbour JA, Poulos RC, Katainen R, Aaltonen LA, Wong JWH. Mutational
668 processes of distinct POLE exonuclease domain mutants drive an enrichment of a specific
669 TP53 mutation in colorectal cancer. PLoS Genet. 2020;16(2):e1008572. Epub 2020/02/06.

doi: 10.1371/journal.pgen.1008572. PubMed PMID: 32012149; PubMed Central PMCID: PMCPMC7018097.

36. Poulos RC, Olivier J, Wong JWH. The interaction between cytosine methylation and processes of DNA replication and repair shape the mutational landscape of cancer genomes. Nucleic Acids Research. 2017;45(13):7786-95. doi: 10.1093/nar/gkx463.

37. Tomkova M, McClellan M, Kriaucionis S, Schuster-Böckler B. DNA Replication and associated repair pathways are involved in the mutagenesis of methylated cytosine. DNA Repair. 2018;62:1-7. doi: 10.1016/j.dnarep.2017.11.005.

38. Behringer MG, Hall DW. Genome-Wide Estimates of Mutation Rates and Spectrum in Schizosaccharomyces pombe Indicate CpG Sites are Highly Mutagenic Despite the Absence of DNA Methylation. G3 (Bethesda, Md). 2015;6(1):149-60. doi: 10.1534/g3.115.022129.

39. Farlow A, Long H, Arnoux S, Sung W, Doak TG, Nordborg M, et al. The Spontaneous Mutation Rate in the Fission Yeast Schizosaccharomyces pombe. Genetics. 2015;201(2):737-44. doi: 10.1534/genetics.115.177329.

40. Wood V, Gwilliam R, Rajandream MA, Lyne M, Lyne R, Stewart A, et al. The genome sequence of Schizosaccharomyces pombe. Nature. 2002;415(6874):871-80. Epub 2002/02/23. doi: 10.1038/nature724. PubMed PMID: 11859360.

41. Meier B, Volkova NV, Hong Y, Schofield P, Campbell PJ, Gerstung M, et al. Mutational signatures of DNA mismatch repair deficiency in C. elegans and human cancers. Genome Research. 2018;28(5):666-75. doi: 10.1101/gr.226845.117.

42. Blokzijl F, Janssen R, van Boxtel R, Cuppen E. MutationalPatterns: comprehensive genome-wide analysis of mutational processes. Genome Med. 2018;10(1):33. Epub 2018/04/27. doi: 10.1186/s13073-018-0539-0. PubMed PMID: 29695279; PubMed Central PMCID: PMCPMC5922316.

43. Fleck O, Vejrup-Hansen R, Watson A, Carr AM, Nielsen O, Holmberg C. Spd1 accumulation causes genome instability independently of ribonucleotide reductase activity but functions to protect the genome when deoxynucleotide pools are elevated. Journal of cell science. 2013;126(Pt 21):4985-94. doi: 10.1242/jcs.132837.

44. Gou L, Bloom JS, Kruglyak L. The genetic basis of mutation rate variation in yeast. Genetics. 2019;211(2):731-40. doi: 10.1534/genetics.118.301609.

45. Iyer DR, Rhind N. Replication fork slowing and stalling are distinct, checkpoint-independent consequences of replicating damaged DNA. PLOS Genetics. 2017;13(8):e1006958-e. doi: 10.1371/journal.pgen.1006958.

46. Schmidt TT, Reyes G, Gries K, Ceylan CÜ, Sharma S, Meurer M, et al. Alterations in cellular metabolism triggered by URA7 or GLN3 inactivation cause imbalanced dNTP pools and increased mutagenesis. Proceedings of the National Academy of Sciences of the United States of America. 2017;114(22):E4442-E51. doi: 10.1073/pnas.1618714114.

47. Pai CC, Kearsey S. A Critical Balance: dNTPs and the Maintenance of Genome Stability. Genes. 2017;8(2):57-. doi: 10.3390/genes8020057.

48. Azvolinsky A, Dunaway S, Torres JZ, Bessler JB, Zakian VA. The S. cerevisiae Rrm3p DNA helicase moves with the replication fork and affects replication of all yeast chromosomes. Genes & development. 2006;20(22):3104-16. doi: 10.1101/gad.1478906.

49. Gagou ME, Ganesh A, Phear G, Robinson D, Petermann E, Cox A, et al. Human PIF1 helicase supports DNA replication and cell growth under oncogenic-stress. Oncotarget. 2014;5(22):11381-98. doi: 10.18632/oncotarget.2501.

50. McDonald KR, Guise AJ, Pourbozorgi-Langroudi P, Cristea IM, Zakian VA, Capra JA, et al. Pfh1 Is an Accessory Replicative Helicase that Interacts with the Replisome to Facilitate

Fork Progression and Preserve Genome Integrity. PLOS Genetics. 2016;12(9):e1006238-e. doi: 10.1371/journal.pgen.1006238.

51. Pinter SF, Aubert SD, Zakian VA. The Schizosaccharomyces pombe Pfh1p DNA Helicase Is Essential for the Maintenance of Nuclear and Mitochondrial DNA. Molecular and Cellular Biology. 2008;28(21):6594-608. doi: 10.1128/MCB.00191-08.

52. Audry J, Maestroni L, Delagoutte E, Gauthier T, Nakamura TM, Gachet Y, et al. RPA prevents G-rich structure formation at lagging-strand telomeres to allow maintenance of chromosome ends. The EMBO journal. 2015;34(14):1942-58. doi: 10.15252/embj.201490773.

53. van Gool IC, Bosse T, Church DN. POLE proofreading mutation, immune response and prognosis in endometrial cancer. Oncoimmunology. 2016;5(3):e1072675. Epub 2016/05/04. doi: 10.1080/2162402X.2015.1072675. PubMed PMID: 27141333; PubMed Central PMCID: PMCPMC4839358.

54. Li HD, Lu C, Zhang H, Hu Q, Zhang J, Cuevas IC, et al. A PoleP286R mouse model of endometrial cancer recapitulates high mutational burden and immunotherapy response. JCI Insight. 2020;5(14). Epub 2020/07/24. doi: 10.1172/jci.insight.138829. PubMed PMID: 32699191; PubMed Central PMCID: PMCPMC7453891.

55. Washington MT, Johnson RE, Prakash L, Prakash S. Human DINB1-encoded DNA polymerase kappa is a promiscuous extender of mispaired primer termini. Proc Natl Acad Sci U S A. 2002;99(4):1910-4. Epub 2002/02/14. doi: 10.1073/pnas.032594399. PubMed PMID: 11842189; PubMed Central PMCID: PMCPMC122293.

56. Johnson RE, Prakash S, Prakash L. The human DINB1 gene encodes the DNA polymerase Poltheta. Proc Natl Acad Sci U S A. 2000;97(8):3838-43. Epub 2000/04/13. doi: 10.1073/pnas.97.8.3838. PubMed PMID: 10760255; PubMed Central PMCID: PMCPMC18103.

57. Tonzi P, Yin Y, Lee CWT, Rothenberg E, Huang TT. Translesion polymerase kappa-dependent DNA synthesis underlies replication fork recovery. Elife. 2018;7. Epub 2018/11/14. doi: 10.7554/eLife.41426. PubMed PMID: 30422114; PubMed Central PMCID: PMCPMC6251625.

58. Bulock CR, Xing X, Shcherbakova PV. Mismatch repair and DNA polymerase delta proofreading prevent catastrophic accumulation of leading strand errors in cells expressing a cancer-associated DNA polymerase variant. Nucleic Acids Res. 2020;48(16):9124-34. Epub 2020/08/07. doi: 10.1093/nar/gkaa633. PubMed PMID: 32756902; PubMed Central PMCID: PMCPMC7498342.

59. Barnes RP, Hile SE, Lee MY, Eckert KA. DNA polymerases eta and kappa exchange with the polymerase delta holoenzyme to complete common fragile site synthesis. DNA Repair. 2017;57:1-11. doi: 10.1016/j.dnarep.2017.05.006.

60. Prindle MJ, Fox EJ, Loeb LA. The mutator phenotype in cancer: molecular mechanisms and targeting strategies. Current drug targets. 2010;11(10):1296-303. doi: 10.2174/1389450111007011296.

61. Fox EJ, Loeb LA. Lethal mutagenesis: targeting the mutator phenotype in cancer. Seminars in cancer biology. 2010;20(5):353-9. doi: 10.1016/j.semcancer.2010.10.005.

62. Rentoft M, Lindell K, Tran P, Chabes AL, Buckland RJ, Watt DL, et al. Heterozygous colon cancer-associated mutations of SAMHD1 have functional significance. Proceedings of the National Academy of Sciences of the United States of America. 2016;113(17):4723-8. doi: 10.1073/pnas.1519128113.

763 63. Cerami E, Gao J, Dogrusoz U, Gross BE, Sumer SO, Aksoy BA, et al. The cBio cancer
764 genomics portal: an open platform for exploring multidimensional cancer genomics data.
765 Cancer Discov. 2012;2(5):401-4. Epub 2012/05/17. doi: 10.1158/2159-8290.CD-12-0095.
766 PubMed PMID: 22588877; PubMed Central PMCID: PMCPMC3956037.
767 64. Gao J, Aksoy BA, Dogrusoz U, Dresdner G, Gross B, Sumer SO, et al. Integrative
768 analysis of complex cancer genomics and clinical profiles using the cBioPortal. Sci Signal.
769 2013;6(269):pl1. Epub 2013/04/04. doi: 10.1126/scisignal.2004088. PubMed PMID:
770 23550210; PubMed Central PMCID: PMCPMC4160307.
771 65. Moreno S, Klar A, Nurse P. Molecular genetic analysis of fission yeast
772 Schizosaccharomyces pombe. Methods Enzymol. 1991;194:795-823. Epub 1991/01/01. doi:
773 10.1016/0076-6879(91)94059-l. PubMed PMID: 2005825.
774 66. Guarino E, Shepherd ME, Salguero I, Hua H, Deegan RS, Kearsey SE. Cdt1 proteolysis
775 is promoted by dual PIP degrons and is modulated by PCNA ubiquitylation. Nucleic Acids
776 Res. 2011;39(14):5978-90. Epub 2011/04/16. doi: 10.1093/nar/gkr222. PubMed PMID:
777 21493688; PubMed Central PMCID: PMCPMC3152358.
778 67. Pai CC, Hsu KF, Durley SC, Keszthelyi A, Kearsey SE, Rallis C, et al. An essential role for
779 dNTP homeostasis following CDK-induced replication stress. J Cell Sci. 2019;132(6). Epub
780 2019/01/25. doi: 10.1242/jcs.226969. PubMed PMID: 30674555; PubMed Central PMCID:
781 PMCPMC6451416.
782 68. Aoude LG, Heitzer E, Johansson P, Gartside M, Wadt K, Pritchard AL, et al. POLE
783 mutations in families predisposed to cutaneous melanoma. Fam Cancer. 2015;14(4):621-8.
784 Epub 2015/08/08. doi: 10.1007/s10689-015-9826-8. PubMed PMID: 26251183.
785 69. Palles C, Cazier JB, Howarth KM, Domingo E, Jones AM, Broderick P, et al. Germline
786 mutations affecting the proofreading domains of POLE and POLD1 predispose to colorectal
787 adenomas and carcinomas. Nat Genet. 2013;45(2):136-44. Epub 2012/12/25. doi:
788 10.1038/ng.2503. PubMed PMID: 23263490; PubMed Central PMCID: PMCPMC3785128.
789 70. Goldsby RE, Hays LE, Chen X, Olmsted EA, Slayton WB, Spangrude GJ, et al. High
790 incidence of epithelial cancers in mice deficient for DNA polymerase delta proofreading.
791 Proc Natl Acad Sci U S A. 2002;99(24):15560-5. Epub 2002/11/14. doi:
792 10.1073/pnas.232340999. PubMed PMID: 12429860; PubMed Central PMCID:
793 PMCPMC137756.
794 71. Ralph E, Boye E, Kearsey SE. DNA damage induces Cdt1 proteolysis in fission yeast
795 through a pathway dependent on Cdt2 and Ddb1. EMBO Rep. 2006;7(11):1134-9. Epub
796 2006/10/14. doi: 10.1038/sj.embor.7400827. PubMed PMID: 17039252; PubMed Central
797 PMCID: PMCPMC1679788.
798 72. Manjon E, Edreira T, Munoz S, Sanchez Y. Rgf1p (Rho1p GEF) is required for double-
799 strand break repair in fission yeast. Nucleic Acids Res. 2017;45(9):5269-84. Epub
800 2017/03/24. doi: 10.1093/nar/gkx176. PubMed PMID: 28334931; PubMed Central PMCID:
801 PMCPMC5435928.
802 73. Pedregosa F, Varoquaux G, Gramfort A, Michel V, Thirion B, Grisel O, et al. Scikit-
803 learn: Machine Learning in {P}ython. Journal of Machine Learning Research2011. p. 2825-30.
804 74. Kearsey SE, Brimage L, Namdar M, Ralph E, Yang X. In situ assay for analyzing the
805 chromatin binding of proteins in fission yeast. Methods Mol Biol. 2005;296:181-8. Epub
806 2004/12/04. doi: 10.1385/1-59259-857-9:181. PubMed PMID: 15576932.
807 75. Hua H, Namdar M, Ganier O, Gregan J, Mechali M, Kearsey SE. Sequential steps in
808 DNA replication are inhibited to ensure reduction of ploidy in meiosis. Mol Biol Cell.

2013;24(5):578-87. Epub 2013/01/11. doi: 10.1091/mbc.E12-11-0825. PubMed PMID: 23303250; PubMed Central PMCID: PMCPMC3583662.

76. Bianco JN, Poli J, Saksouk J, Bacal J, Silva MJ, Yoshida K, et al. Analysis of DNA replication profiles in budding yeast and mammalian cells using DNA combing. Methods. 2012;57(2):149-57. Epub 2012/05/15. doi: 10.1016/j.ymeth.2012.04.007. PubMed PMID: 22579803.

Figure legends

Figure 1

The *POLE-P286R* hypermutagenic phenotype is conserved in *S. pombe*.

A) Multiple sequence alignment showing that the Pro286 residue (red) adjacent to the Exo I domain (blue shadow) is absolutely conserved in Pol ε and Pol δ orthologues as well as in T4 and RB69 phage polymerases. Catalytic residues of the 3'->5' exonuclease domain are highlighted in magenta.

B) CanR mutation rates of *pol2-P287R*, *pol3-P311R* (equivalent proline to Pol2-P287), and exonull Pol2 and Pol3 relative to wild type. A multiple comparison using the ordinary one-way ANOVA revealed that the *pol2-P287R* strain has a significantly greater mutation rate compared to wild-type (black asterisks, *** $P<0.0001$) and *pol2-D276A/E278A* (exonull) (grey asterisks, ** $P<0.01$).

C) Number of base substitutions and frameshift identified in the mutation accumulation (MA) experiment in wild-type, exonull and *pol2-P287R* cells. To accommodate the possibility that suppressor mutations would arise in the *pol2-P287R* strain, three lineages were set up for this strain and the average number of mutations is shown.

D) Expected and observed distribution of mutations obtained in *pol2-P287R* cells during the MA experiment across different genomic regions.

Figure 2

Mutational spectra of the P286R variant in human adenocarcinomas and *S. pombe.*

A) Mutation types in *POLE-P286R* colorectal carcinoma (top) and uterine endometrioid carcinoma (bottom).

B) Mutation types in *pol2-P287R* (top) and wild-type (bottom) [38] *S. pombe*.

C) Base composition in the vicinity of mutations in *pol2-P287R* and wild-type genomes.

D) Percentage of TCT>TAT in AT-rich sequences in *S. pombe pol2-P287R, POLE-P286R* colorectal carcinoma, and *POLE-P286R* uterine endometrioid carcinoma.

Figure 3

Comparison between *S. pombe* mutational patterns and human cancer signatures.

A) Base substitution patterns of *S. pombe pol2-P287R* and wild-type strains and their corresponding humanized versions (mirrored).

B) Heatmap of cosine similarities between the fission yeast mutational profiles and COSMIC signature. The signatures have been ordered according to hierarchical clustering using the cosine similarity between signatures, such that similar signatures are displayed close together.

C) Comparison between COSMIC signature 14 (SBS14) and *pol2-P287R* humanized profile.

Figure 4

The *pol2-P287R* strain is sensitive to DNA-damaging agents and increased dNTP levels.

A) Spot assays to assess sensitivity to DNA-damaging agents of wild-type, exonull and *pol2-P287R* strains. 1:5 serial dilutions of the indicated strains were spotted on YES plates supplemented with 0.3 and 0.5 μg/ml Bleocin, 0.5 μM 4-NQO, 0.01% MMS, 7.5 mM HU or no drug and incubated at 26° or 30°C for 2-3 days.

B) dNTP levels of the indicated strains measured from samples of exponential growing cells. Means ± SEs of three experiments are shown. The *cdc22-D57N* mutant, where allosteric regulation of RNR is inactivated, is shown as a positive control.

C) Tetrad dissection of genetic crosses of between *cdc22-D57N* and *pol2* mutants. Representative spores from four asci are shown for each cross.

Figure 5

S. pombe pol2-P287R cells show growth and S phase defects and DNA damage checkpoint activation.

A) Growth rate of wild-type, exonuclease and *pol2-P287R* cells. Growth curves for the strains indicated were obtained by absorbance measurements every 20 minutes for 22h. The growth curves are representative of 3 independent experiments. **** P<0.0001.

B) S phase progression in wild-type, exonull and *pol2-P287R* cells. Cells were arrested in G1 phase by nitrogen starvation, then refed and progress of S phase was monitored by flow cytometry.

C) DNA combing analysis of replication tracks in wild-type and *pol2-P287R S. pombe* cells. Strains used were modified to allow uptake of EdU. Cells were pulsed with 100 μM EdU for 15 min, then DNA was combed and EdU was detected using fluorescently-tagged AlexaFluor 488 Azide.

D) Quantitative analysis of track lengths from experiment described in (C)

E) Spot testing of *rad3ts* strains. Serial dilutions of the indicated *S. pombe* strains were spotted to YES plates and incubated at the indicated temperatures.

F) Percentage of RPA foci in unstressed wild-type, exonull and *pol2-P287R* cells. Cells from the indicated strains were cultured to midlog phase in YES medium and imaged live. The numbers of foci in at least 350 nuclei were scored in three independent experiments, and mean values were plotted with error bars representing the standard deviation of the mean. *** P<0.0001 (Student's t-test)

G) Analysis of Chk1 phosphorylation in wild-type, exonull and *pol2-P287R* cells. Chk1-HA strains were grown to log phase and protein extracts were analysed by western blotting. Wild-type cells grown in 0.025% MMS is shown as a positive control.

H) Analysis of Cds1-HA phosphorylation in unstressed wild-type and *pol2-P287R* cells. Wild-type cells grown in YES + 10 mM HU is shown as a positive control. Protein extracts were analysed by western blotting. α- tubulin was used as a loading control.

889 Figure 6

890 Genetic interaction between *pol2-P287R* and *pfh1*.

891 A) *nmt1-pfh1* cells were cultured to midlog phase in minimum medium containing 15 µM
892 thiamine, or no thiamine and imaged live. Representative pictures under unrepressed (-Thi)
893 or *pfh1* repression (+Thi) are shown.

894 B) 1:5 serial dilutions of the indicated strains were spotted onto minimum medium plus or
895 minus thiamine and incubated 3 days at 26°, 30° and 36°C.

896 C) As (B) except cells were spotted onto plates containing 0.5 µM 4-NQO, 0.01% MMS or no
897 drug.

898 Figure 7

899 Deletion of the TLS Pol κ and η genes reduces the mutation rate of *pol2-P287R* cells.

900 A) Can^R mutation rates of the indicated strains relative to wild type, determined by
901 fluctuation analysis.

902 B) Number of base substitutions and frameshift mutations during 200 MA experiments in
903 single and double polymerase mutants. The horizontal grey line shows the average number
904 of SNPs in the *pol2-P287R* strain from Fig. 1C. Single 200 generation lineages were analysed
905 and the total numbers of SNPs/indels found in the 200 generation data relative to the
906 reference sequence but not in the 0 generation data are shown.

907

908

A

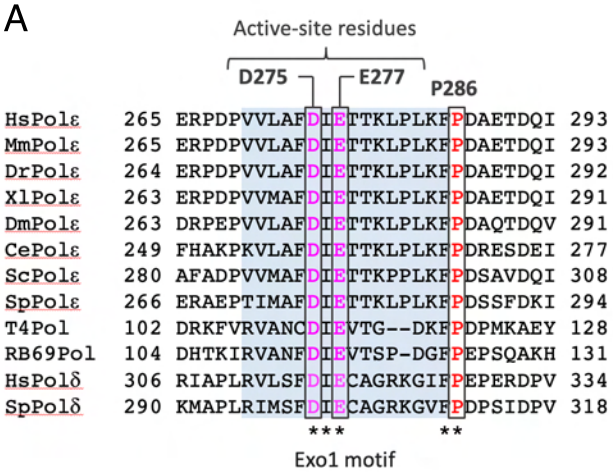

B

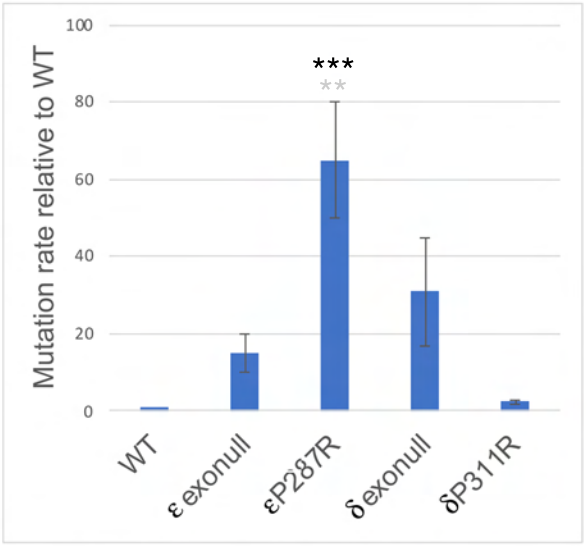

C

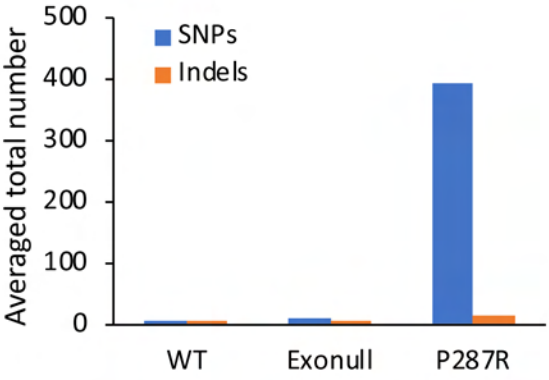

D

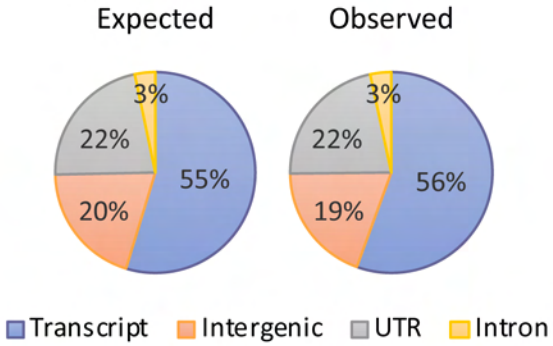

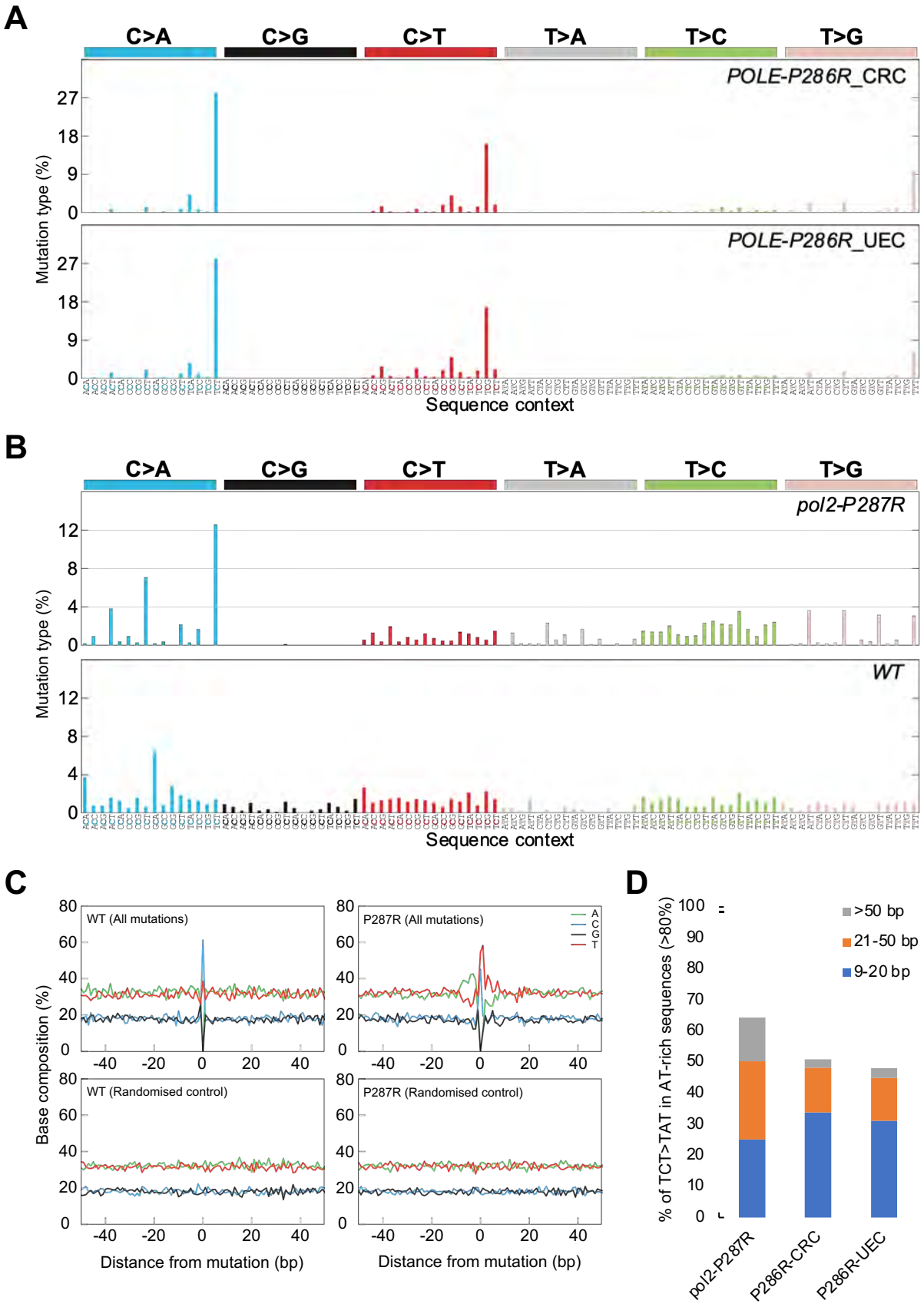
A
C>A
C>G
C>T
T>A
T>C
T>G
POLE-P286R_CRC
POLE-P286R_UEC
Mutation type (%)
Sequence context
B
pol2-P287R
WT
C
WT (All mutations)
P287R (All mutations)
WT (Randomised control)
P287R (Randomised control)
Base composition (%)
Distance from mutation (bp)
D
% of TCT>TAT in AT-rich sequences (>80%)
>50 bp
21-50 bp
9-20 bp
pol2-P287R
P286R-CRC
P286R-UEC

Fig. 2

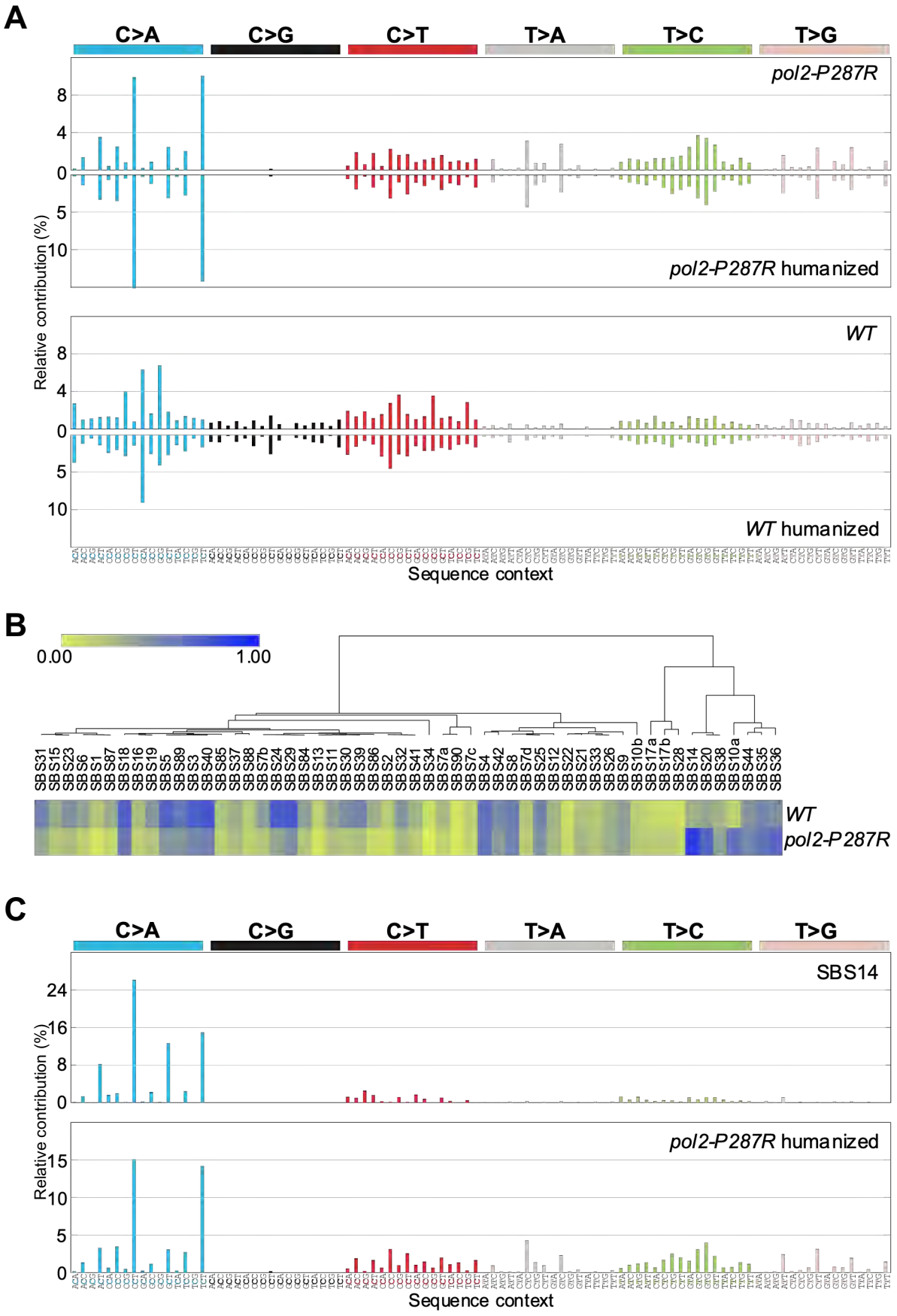
A
C>A
C>G
C>T
T>A
T>C
T>G
pol2-P287R
pol2-P287R humanized
WT
WT humanized
Relative contribution (%)
Sequence context
B
0.00
1.00
SBS31 SBS15 SBS23 SBS6 SBS1 SBS87 SBS18 SBS16 SBS19 SBS5 SBS89 SBS3 SBS40 SBS85 SBS37 SBS88 SBS7b SBS24 SBS29 SBS84 SBS13 SBS11 SBS30 SBS39 SBS86 SBS2 SBS32 SBS41 SBS34 SBS7a SBS90 SBS7c SBS4 SBS42 SBS8 SBS7d SBS25 SBS12 SBS22 SBS21 SBS33 SBS26 SBS9 SBS10b SBS17a SBS17b SBS28 SBS14 SBS20 SBS38 SBS10a SBS44 SBS35 SBS36
WT
pol2-P287R
C
C>A
C>G
C>T
T>A
T>C
T>G
SBS14
pol2-P287R humanized
Relative contribution (%)
Sequence context

Fig. 3

A

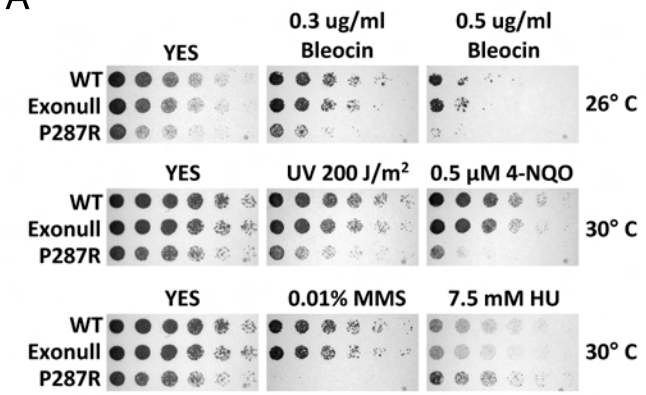

B

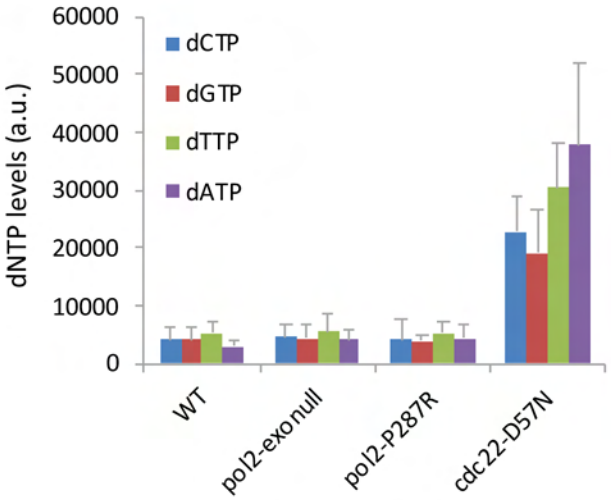

C

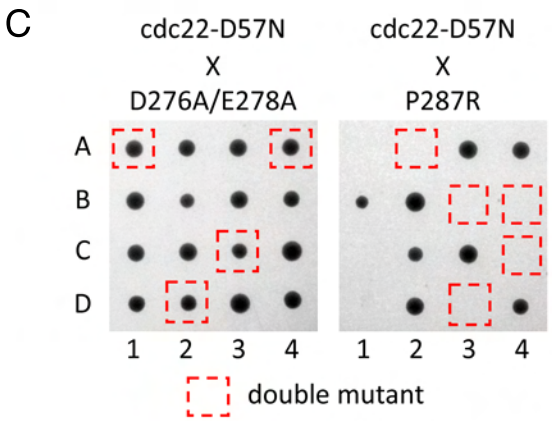

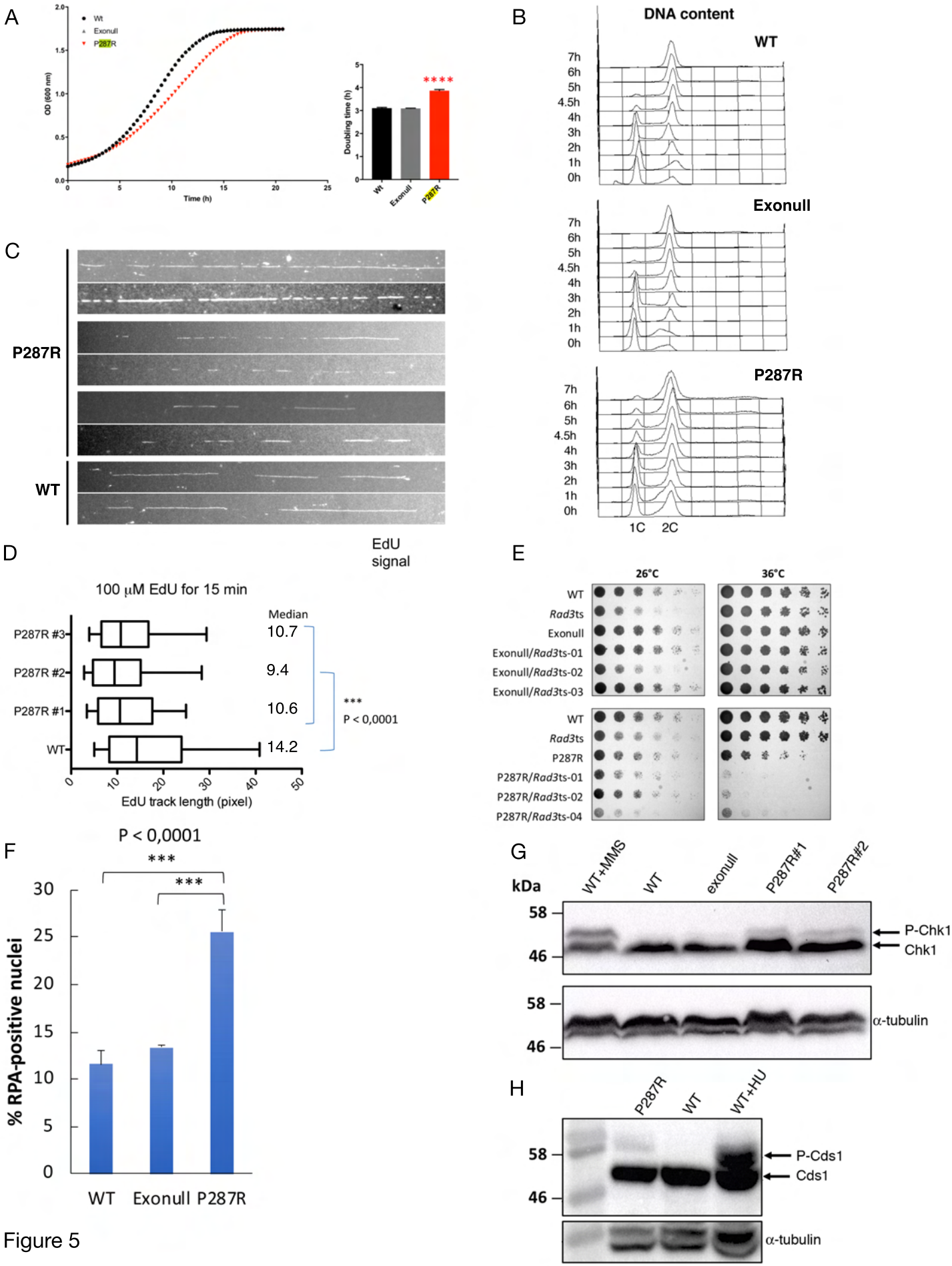
A
Wt
Exonull
P287R
OD (600 nm)
Time (h)
Doubling time (h)
****
Wt
Exonull
P287R
B
DNA content
WT
Exonull
P287R
7h
6h
5h
4.5h
4h
3h
2h
1h
0h
1C
2C
C
P287R
WT
EdU signal
D
100 μM EdU for 15 min
Median
P287R #3
P287R #2
P287R #1
WT
10.7
9.4
10.6
14.2
***
P < 0,0001
EdU track length (pixel)
E
26°C
36°C
WT
Rad3ts
Exonull
Exonull/Rad3ts-01
Exonull/Rad3ts-02
Exonull/Rad3ts-03
WT
Rad3ts
P287R
P287R/Rad3ts-01
P287R/Rad3ts-02
P287R/Rad3ts-04
F
P < 0,0001
***
***
% RPA-positive nuclei
WT
Exonull
P287R
G
kDa
WT+MMS
WT
exonull
P287R#1
P287R#2
58
46
P-Chk1
Chk1
α-tubulin
H
P287R
WT
WT+HU
P-Cds1
Cds1
α-tubulin

Figure 5

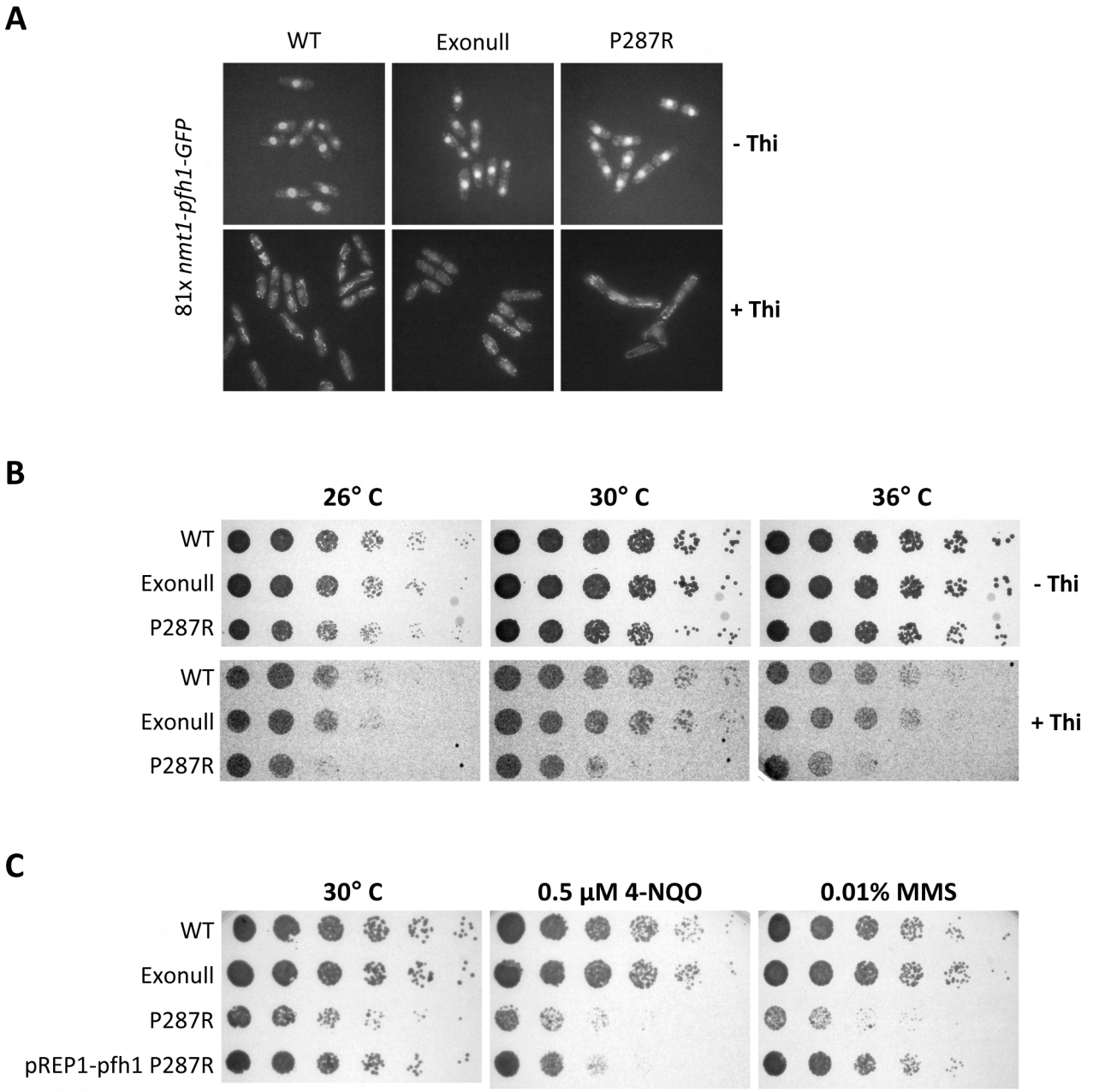
A
WT
Exonull
P287R
81x nmt1-pfh1-GFP
- Thi
+ Thi
B
26° C
30° C
36° C
WT
Exonull
P287R
- Thi
WT
Exonull
P287R
+ Thi
C
30° C
0.5 µM 4-NQO
0.01% MMS
WT
Exonull
P287R
pREP1-pfh1 P287R

Fig. 6

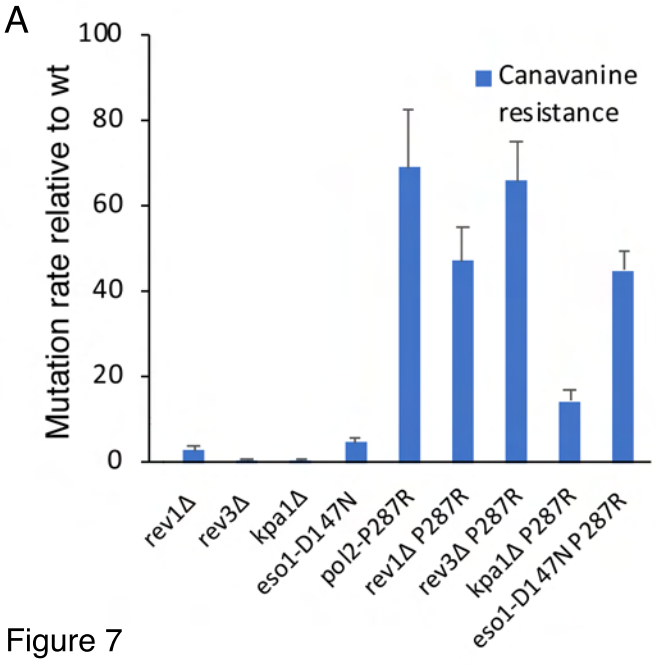
A
Mutation rate relative to wt
100
80
60
40
20
0
Canavanine resistance
rev1Δ
rev3Δ
kpa1Δ
eso1-D147N
pol2-P287R
rev1Δ P287R
rev3Δ P287R
kpa1Δ P287R
eso1-D147N P287R

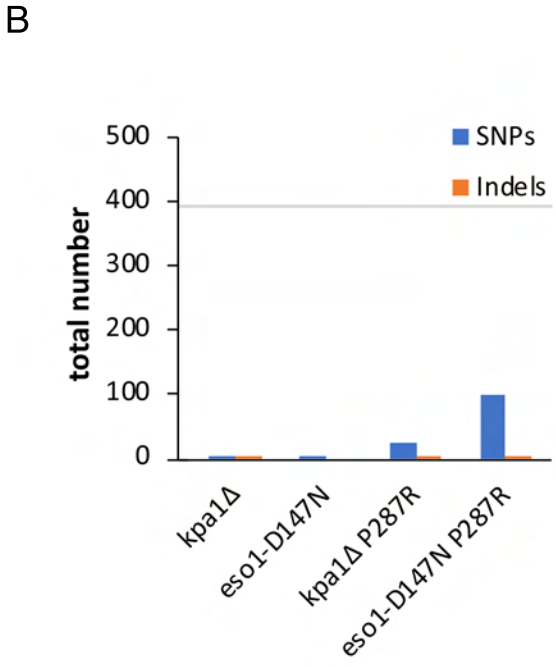
B
total number
500
400
300
200
100
0
SNPs
Indels
kpa1Δ
eso1-D147N
kpa1Δ P287R
eso1-D147N P287R

Figure 7